PCCP

PAPER

View Article Online
View Journal | View Issue

Cite this: *Phys. Chem. Chem. Phys.*, 2025, **27**, 20368

Adsorption modes of cysteine on gold: from neutral molecules to unconventional zwitterions

Clayton B. Smith,[a] Aishat Idris,[a] Elvis C. M. Ting[a] and Irina Paci *[ab]

The adsorption of amino acids on coinage metal surfaces is of interest for a range of biological applications. Central to advancing these applications is understanding the structure of the adsorbed molecules and the state they are present in. Cysteine, the focus of this work, has been studied extensively, both experimentally and theoretically. Here, density functional theory (DFT) and DFT-driven molecular dynamics are used to examine the different adsorption modes of the cysteine monomer on an Au(111) surface in vacuum. Dimeric structures and their influence on the adsorption mode of the individual molecules are also considered. We find that the most stable monomeric binding mode is an unconventional zwitterion with the ammonium group formed by donation of the mercapto hydrogen. Moreover, we observe the transformation of neutral adsorbed molecules to unconventional zwitterions through direct or indirect proton transfer. Conventional zwitterions are unstable in monomeric form, either in gas phase or adsorbed structure calculations.

Received 20th May 2025,
Accepted 26th August 2025

DOI: 10.1039/d5cp01901j

rsc.li/pccp

1 Introduction

The deposition of thiol-containing compounds on gold surfaces has seen considerable interest[1–4] due to their array of envisioned applications, including biosensors,[2] catalysis,[5] and the fabrication of nanoscale devices.[1,3,4] The only proteinogenic amino acid containing a mercapto group, cysteine[4] is involved in the binding of proteins and peptides to metallic substrates. Its deposition on Au and Ag substrates has been explored to gain understanding of amino acid and protein binding on these metals.[6–22] Moreover, when used as a protective ligand, *R*- or *S*-cysteine deposition can direct Au nanoparticle formation and properties,[23–26] including the synthesis of chiral plasmonic nanostructures.[27,28]

Much of the experimental work on the vacuum adsorption of cysteine has focused on pattern formation in self-assembled structures and their emerging properties. In terms of monomer adsorption, using X-ray photoelectron spectroscopy, Canepa *et al.*[11,12] found that the cysteine molecule lies flat on the Au(110) surface and adsorbs to the Au(110) and Au(111) surfaces through the thiol group.

One outstanding problem in the study of the cysteine–gold system is the structure of the adsorbed cysteine molecule. In experimental investigations, it appears that the amino group is in a NH_3^+ state when adsorbed on both Au(110)[12] and Au(111)[10,29,30] surfaces. The charged state of cysteine was suggested based on several experimental techniques, including temperature programmed desorption, X-ray photoelectron spectroscopy and mass spectrometry.[10] Scanning tunnelling microscopy of Au(111)-deposited cysteine by Kühnle and coworkers[7] found structurally distinct monolayer patches, suggesting the molecules acquire a variety of bonding and charging states after deposition. At lower densities, on Au(110) reconstructed substrates, homochiral dimers or octamers form on the surface and the molecules appear to be neutral.[8,9,31] Further experimental studies have looked at the structure of cysteine adsorbed in aqueous conditions[10,29,30,32–37] or its structure within larger self-assembled structures.[38] Many of these studies also found evidence of chemisorption.[29,30,32,33,37,38]

While much of the previous theoretical work has considered an adsorption mode that includes a thiolate–gold bond (resulting from the dissociation of the hydrogen of the thiol group),[16,18,39] others have also compared this with a neutral cysteine binding mode.[13,17] Zwitterionic forms of cysteine, by comparison, have received significantly less attention, and studies that have looked at zwitterionic cysteine have focused on a NH_3^+/COO^- zwitterion with a dissociated thiolate headgroup.[10,40,41]

Besides the need for further research, these data suggest a variety of adsorption modes of cysteine on metallic substrates, depending on deposition conditions and substrate facets. Here, we examine the relative stability of the different adsorbed forms of cysteine monomers on the Au(111) surface: undissociated thiol, thiolate, zwitterionic thiol. Additionally, an unconventional ($S^-/NH_3^+/COOH$) zwitterionic form of cysteine has been previously observed experimentally on TiO_2 surfaces.[42] Its possible existence

[a] *Department of Chemistry, University of Victoria, Victoria, BC V8W 2Y2, Canada. E-mail: ipaci@uvic.ca*
[b] *Centre for Advanced Materials and Related Technologies, University of Victoria, Victoria, BC, Canada*

and relative stability on Au(111) substrates will be a focus of this work.

By and large, previous theoretical studies of the adsorption of cysteine on gold surfaces have used density functional theory (DFT) calculations.[13–15,17–19] However, given the complex potential energy surface, simple DFT geometry optimizations can be trapped near their initial, user-input configurations. To more broadly explore the configurational space of the adsorbate on the surface, we investigate several distinct adsorption motifs in a variety of initial structures, using Born Oppenheimer molecular dynamics (BOMD) with a room-temperature thermostat. Besides providing thermal energy to overcome barriers between local minima, BOMD can facilitate chemical reactions such as proton transfer, by overcoming reaction barriers in relatively simple cases.

We show that the unconventional zwitterionic form appears to be the most stable motif for cysteine monomers and dimers adsorbed at the Au(111) ideal surface. Moreover, other optimized motifs such as the uncharged molecule will undergo proton transfer to transform to this motif at room temperatures. Unconventional zwitterions and uncharged molecules present competitive adsorbed configurations with relatively low conversion barriers. These results provide a theoretical basis for the multitude of adsorbed configurations observed experimentally in cysteine adsorption at low and medium coverages on Au surfaces.

2 Models and methods

2.1 Molecule and surface models

An 168-atom, 20.59 Å × 20.34 Å periodic Au(111) 3-layer slab was used throughout the work presented here. Slabs were generated starting with the Import .cif file utility in Avogadro 1.2,[43] which uses a variety of crystalline structure databases, including, in this case, the American Mineralogist Crystal Structure Database.[44,45] The primitive cell was optimized to the theoretical GGA potential using variable-cell periodic boundary conditions. A 3-layer slab was generated from the optimized structure, then re-optimized as a slab while keeping the bottom layer and cell dimensions frozen. To mimic adsorption on a crystalline surface, the bottom layer of surface atoms was held fixed at the optimized bulk coordinates in all calculations, and the remaining atoms were allowed to optimize. This was done to help the slab maintain its general structure while still enabling realistic surface–adsorbate interactions by having the upper two layers unfixed. A vacuum padding bringing the periodic cell length to 100 Å in the z direction prevented interactions between periodic images in this direction. Lateral interactions between adsorbates residing in image cells are also reduced, due to the relatively large slab size. The large cell dimensions minimize the size of the Brillouin zone, allowing for calculations to be performed at the Γ point only.

Four distinct adsorption modes were considered for the adsorbate: neutral cysteine, conventional zwitterionic (COO^-/NH_3^+), uncoventional zwitterionic (S^-/NH_3^+), and thiolate (S^-). A number of the initial geometries for neutral cysteine had their functional groups oriented so as to encourage formation of one of the two zwitterionic species. Dimer structures were also explored with a variety of initial structures based on combinations of unconventional zwitterionic and neutral molecules.

2.2 Calculation details

Calculations were performed using the SIESTA program,[46] which offers implementations of DFT optimizations using a conjugate gradient (CG) approach and DFT-based BOMD with periodic boundary conditions. Conjugate gradient calculations were used primarily to locally optimize geometries and calculate relative electronic energies. These types of calculations are often unable to sample the configurational space, and are known to become trapped close to the initial configurations provided as input. This is particularly problematic on complex potential energy surfaces, such as those occurring in molecule–surface interactions.[47] Moreover, classical simulations, including Monte Carlo and classical MD, suffer from the problematic treatment of the S–Au interaction and structure by the classical potential.[16,48] Here, we use BOMD calculations at a temperature of 300 K to sample the configurational space beyond the restrictive sampling provided by the conjugate gradient methodolgy. Thermal energy and thermal fluctuations allow the system to overcome local barriers in these calculations, even though computationally feasible runtimes do not allow for full equilibration and statistical interpretation of the simulation results. A subset of 10–20 low-energy geometries generated by the BOMD simulations were extracted for each system, then optimized using DFT to obtain the energies reported in this paper. BOMD simulations were initiated at 150 K ramping up to 300 K, using a Nose thermostat and 1 fs timesteps. The generalized mass of the Nose variable was held at the default 100 Ry fs^2. Simulation times of up to 10 ps were explored.

All calculations used a Perdew–Burke–Ernzerhof functional[49] with Tkachenko–Sheffler[50] screened van der Waals dispersion corrections (PBE–TS-vdW). Core electrons were described in terms of Troullier–Martins pseudopotentials[51] with relativistic corrections for the gold atoms. Valence electrons were described using pseudo-atomic orbitals with a polarized triple-ζ (TZP) basis set. The pseudo-atomic orbitals in SIESTA are strictly localized and fall to zero outside a given cut-off radius, chosen by specifying a value of energy shift. Previous calculations by our group and others[52,53] suggested 1 mRy energy shift (equivalent to 6 Å for the cutoff radius of the carbon orbital with the smallest ζ). Moreover, counterpoise corrections for the basis set superposition error[54] were applied in the calculation of binding energies for the adsorption of neutral molecules.

2.3 Binding energies

The binding energies reported in the following pages are calculated from CG-optimized energies, based on the specifics of the adsorption process. For complexes obtained through the dissociation of the thiol group on the surface (non-zwitterionic thiolates and conventional zwitterions with thiolate binding),

binding energies were calculated as the reaction energies for dissociative adsorption:

$$E_b = E_{complex} + \frac{1}{2}E_{H_2} - E_{surf} - E_{mol} \quad (1)$$

where E_{mol}, E_{surf} and $E_{complex}$ are the total energies of the gas phase neutral molecule, free surface and adsorbed complex, respectively.

For cases where H_2 is not produced (undissociated thiols and unconventional zwitterions, where the hydrogen ion is transferred from the mercapto to the amino group), the reported surface binding energies are:

$$E_b = E_{complex} - E_{surf} - E_{mol} \quad (2)$$

As has been done previously in our group, the counterpoise correction was used to account for basis set superposition errors in cases where the headgroup was intact in the optimized structure.[55,56] For the adsorbed thiol, the counterpoise-corrected binding energy is given by:

$$E_{b,corrected} = E_b - (E_{mol}^{complex} - E_{mol}^{mol} + E_{surf}^{complex} - E_{surf}^{surf}) \quad (3)$$

Here, E_b is the energy calculated in eqn (2), $E_{mol}^{complex}$ and $E_{surf}^{complex}$ are the molecular and surface energies calculated based on their adsorbed complex structures using the basis set functions of the entire adsorbed complex. E_{mol}^{mol} and E_{surf}^{surf} are the molecular and surface energies calculated based on their adsorbed complex structures using their own individual basis set functions.

Dimer binding energies are calculated per monomer, so that the (de)stabilizing effect of dimer formation can be assessed:

$$E_{b,dimer} = \frac{1}{2}[E_{complex} - 2E_{mol} - E_{surf}] \quad (4)$$

where $E_{complex}$ is the energy of the dimer–surface complex. When calculated this way, the effect of the bond between the monomers on the energy is included in the binding energies reported for dimers.

3 Results and discussion

3.1 Stability of gas phase monomers and dimers

In the gas phase, monomeric cysteine is stable only in its neutral form. Multiple initial conformations for zwitterionic monomers were considered and their optimization was attempted. All were found to be unstable, and the calculations failed in a variety of ways: dissociation of the molecule, inability to find an optimal structure over many iterations, and proton transfer. Zwitterionic dimers can be stable in gas phase. Their stability is similar to that of neutral dimers (see Fig. 1).

The availability of multiple groups able to participate in intermolecular interactions leads to polymorphism in cysteine assemblies as small as dimers. Fig. 1 shows some of the most stable gas phase dimer structures, with different binding motifs, optimized from either zwitterionic or neutral initial structures. The zwitterionic dimer shown in Fig. 1(a) experiences weak hydrogen bonding between the charged groups, besides charge–charge interactions (H–O distances between ammonium and carboxylate groups are 1.4 Å with N–H–O angles of roughly 165°).

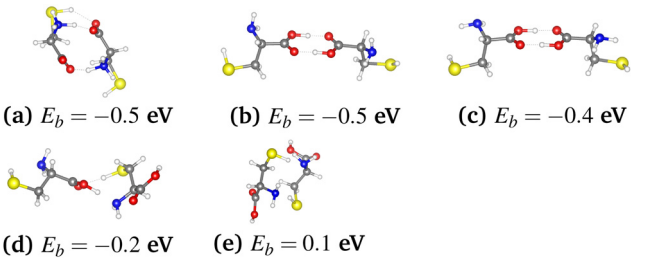

Fig. 1 Examples of CG-optimized gas phase dimer conformations. Panel (a) presents the optimized structure of a zwitterionic dimer. Panels (b)–(e) present various configurations of neutral cysteine dimers. Hydrogen bonding stabilizes the dimers shown in panels (b)–(d) (H–O distances were within 1.81 Å and had bond angles greater than 173° for these structures), whereas the dimer presented in panel (e) is roughly as stable as two non-interacting molecules. Binding energies are shown below the corresponding images. Grey, white, red, blue and yellow atoms represent carbon, hydrogen, oxygen, nitrogen and sulfur, respectively.

The structure is energetically competitive with stable COOH-based hydrogen bonded dimers [Fig. 1(b) and (c)]. In fact, the most important indicator of stability for these structures was the ability of the configuration to form two H-bonds, as single hydrogen bonded complexes such as the one shown in Fig. 1(d) were significantly less stable, and dimers unable to form any hydrogen bonds, such as Fig. 1(e), presented only weak interactions (within the error of the method used). The hydrogen bonding motifs seen in Fig. 1(b) and (c) have been previously described in both experimental and theoretical literature for carboxylic acids,[57–59] and the lengths and angles reported above agree with those in previous works.[59] Hydrogen-bonding motifs involving interactions of the carboxylic group with thiol and amino groups, such as those shown in Fig. 1(a) and (d), have been observed experimentally in the solid phase[60] and theoretically in an aqueous phase.[61]

3.2 Adsorbed monomers

The structural behaviour of Au(111)-deposited cysteine was initially considered by sampling the configuration space of several structural motifs for the adsorbed molecule: neutral-backbone thiolate, neutral thiol (including a mercapto H atom), and zwitterion. Intramolecular proton transfer during optimization of several structures led to an additional structural motif: an ''unconventional'' zwitterionic (abbreviated as U-zwitterion in the following text) structure where the carboxylic group retains its proton, and the ammonium group has received a proton from the thiol. The U-zwitterion emerged as the most stable adsorbed species. Table 1 lists the adsorption energies of the most stable adsorbed monomer conformations obtained in this study. No stable conventional zwitterionic structures were observed. The S–Au distances for the neutral and thiolate structures shown in Table 1 are consistent with previous theoretical calculations,[13–15] as are the adsorption energies for the neutral[13] and thiolate[14,15] structures.

Table 1 Adsorption energies and S–Au distances of cysteine monomers on the Au(111) surface

Motif	Structure[a]	E_b (eV)	d_{S-Au} (Å)
U-zwitterion	Fig. 2(a)	−1.5	(2.47, 3.55)
U-zwitterion	Fig. 2(b)	−1.5	(2.46, 3.71)
U-zwitterion	Fig. 2(c)	−1.5	(2.46, 3.61)
U-zwitterion	Fig. 2(d)	−1.3	(2.48, 3.90)
Neutral	Fig. 3(a)	−1.1	2.53
Neutral	Fig. 3(b)	−1.0	2.58
Neutral	Fig. 3(c)	−0.9	3.74
Neutral	Fig. 3(d)	−0.8	2.61
Neutral	Fig. 3(e)	−0.8	2.61
Neutral	Fig. 3(f)	−0.8	2.69
Thiolate	Fig. 5(a)	−0.5	(2.50, 2.52)
Thiolate	Fig. 5(b)	−0.5	(2.54, 2.59)
Thiolate	Fig. 5(c)	−0.4	(2.47, 2.48)

[a] Structure entries reproduce the panel symbols from Fig. 2 (U-zwitterions), Fig. 3 (neutral cysteine), and Fig. 5 (thiolate).

The primary takeaway from Table 1 and Fig. 2, 3 is that U-zwitterionic motifs are more stable than neutral cysteine motifs. In the geometries investigated, the thiolate headgroup binds at an on-top, at times off-top site, with the carbon backbone and the ammonium group parallel to the surface. Similar flat adsorbed configurations for cysteine were inferred previously from NEXAFS measurements by Cossaro *et al.*[12] The more stable U-zwitterion structures typically have the α-hydrogen facing towards the surface [see Fig. 2(a)–(c)].

Molecules adsorbed in a neutral configuration exhibit a smaller influence of the α-hydrogen – surface interaction (see Table 1 and Fig. 3). In these structures, the entire molecule is parallel to the surface, although overall further from it, and energetic differences between hydrogen-down and hydrogen-up configurations are negligible [see panels (a) and (b) of Fig. 3]. Instead, the lower-energy structures appear to have some degree of intramolecular hydrogen bonding, as seen for example in Fig. 3(a) and (b) (where SH–O interactions had O–H distances below 1.65 Å and bond angles over 152°) or were stabilized by other interactions of the backbone with the surface.

Exhaustive attempts to optimize conventional zwitterionic adsorbates were performed. All such initial geometries either transferred a proton from the ammonium group to the carboxylate group to form a neutral cysteine molecule, or the calculations failed. Four examples of calculations that underwent proton transfer are shown in Fig. 4. We conclude that the adsorbed conventional zwitterion motif is unstable for monomer adsorption in the conditions considered here.

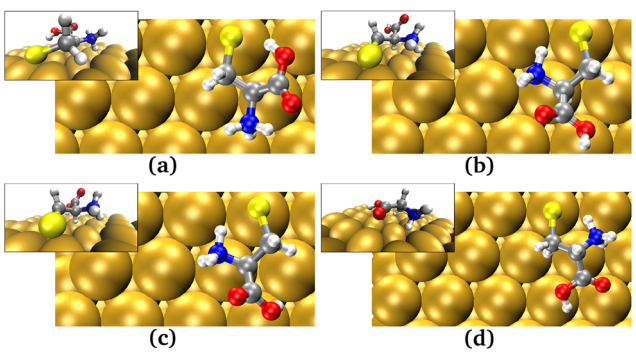

Fig. 2 The four most stable CG-optimized geometries found for the U-zwitterionic binding mode. Panels (a)–(d) present these geometries in order of decreasing binding energy. Respective energies can be found in Table 1.

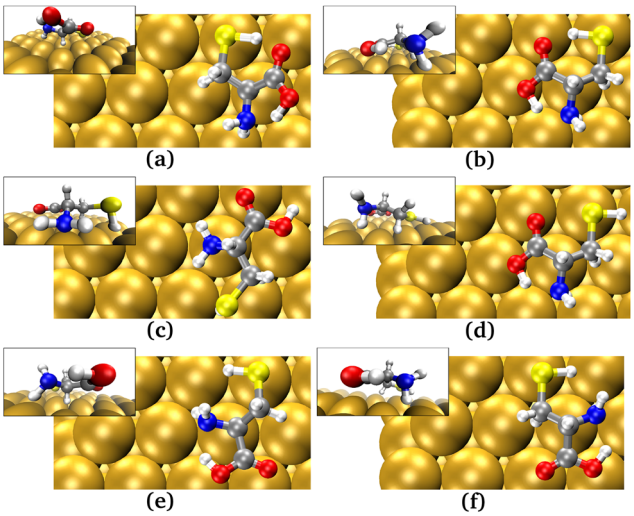

Fig. 3 The most stable CG-optimized geometries found for the neutral cysteine binding mode. Panels (a)–(f) show these geometries in order of decreasing molecule–surface interactions. Respective energies can be found in Table 1.

Thiol adsorption on Au surfaces often occurs through the homolytic dissociation of the mercapto groups,[8,10,13–15] leading to the formation of thiolate motifs. The sulfur's unpaired electron forms a bond to a neighboring gold atom, in addition to a dative bond to another surface atom. Three optimized thiolate structures are shown in Fig. 5, with binding energies included in Table 1. As shown in the table, binding in the thiolate motif was weaker than either the U-zwitterionic or neutral cysteine binding modes. The two-coordinated binding of the headgroup in these structures provides less flexibility for backbone alignment and the binding of the amino group on the surface than in the case of neutral molecule adsorption.[16]

3.3 Electronic structure

The strength of the interaction between the adsorbate and the surface, and ultimately the stability of the complex, are often connected to the density of states (DOS).[62] When projected on the atoms involved in binding, the PDOS of more strongly-bound complexes will show larger distortions from the unbound systems, in conjunction with shifting of antibonding orbitals to higher energies, and above the Fermi level.[17,62,63] Fig. 6(a)–(c) show the DOS projected onto the sulfur, nitrogen and closest-bound gold atoms, respectively, for the unbound and bound systems. Clearer shifts of antibonding orbitals above the Fermi levels are seen for U-zwitterionic and thiolate complexes in the sulfur-projected DOS of Fig. 6(a). Similarly, further distortion of the gold-projected DOS is seen for these systems in Fig. 6(c). The comparison is hampered by the change in electronic structure at the heteroatom due to the unequal

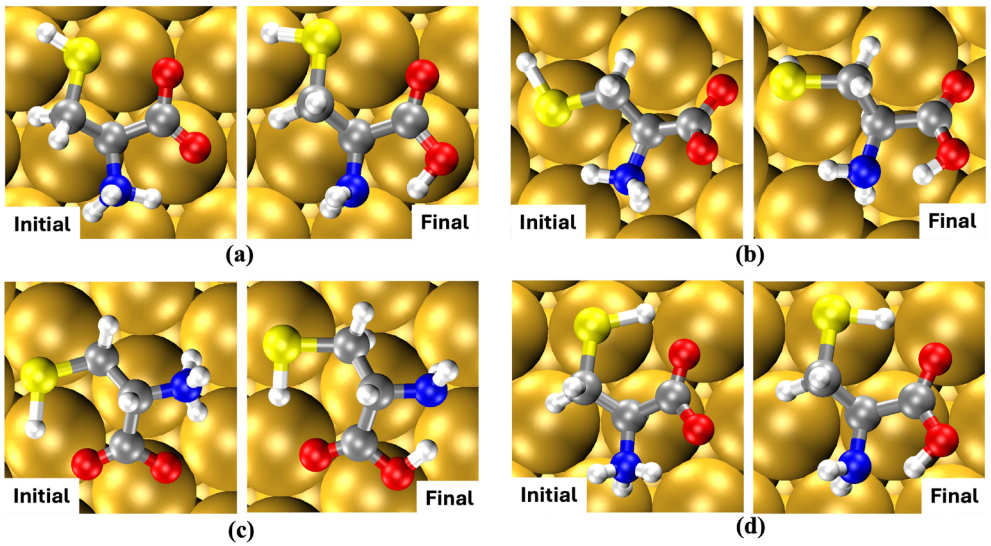

Fig. 4 Initial and final geometries for several conventional zwitterionic forms. All converted to neutral cysteine molecules during geometry optimizations. Distinct conformations of the initial conventional zwitterion are shown in panels (a)–(d), along with the optimized outcomes. None of the structures retain their conventional zwitterionic character in the CG-optimized form.

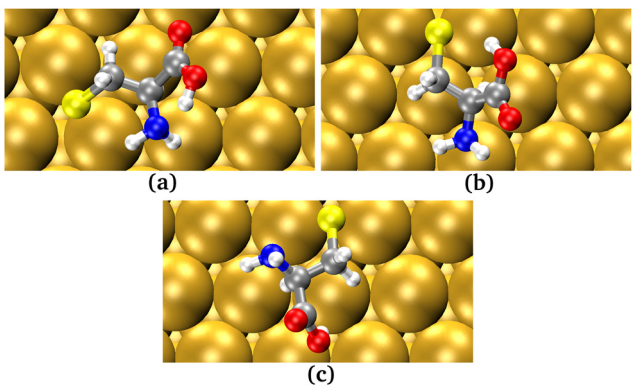

Fig. 5 Stable CG-optimized thiolate motifs for cysteine on the Au(111) surface. Corresponding energies are shown in Table 1. Panels (a)–(c) represent the three most stable distinct geometries found.

number of bound hydrogen atoms. Most discernibly, the nitrogen-projected DOS of the U-zwitterion is mostly flat, as its electronic density is depleted in the formation of the cation. Previous experimental and theoretical work on Au-adsorbed cysteine suggests that the thiol group donates charge density in the Au–S interaction,[11,64–66] although the calculation of small differences in charge using DFT is tenuous.

3.4 Proton transfer

The relative stability of the U-zwitterionic form is further highlighted in BOMD simulations following the neutral cysteine as it reacts with the Au surface. Whereas many such simulations simply follow the molecule as it relaxes on the surface and forms a dative bond with a gold atom, some lead to additional transformations. Two proton transfer pathways have been observed in BOMD simulations or in optimizations.

An indirect proton transfer pathway involves the initial jump of the thiol hydrogen to the carboxylic group. The move is followed by the transfer of the original carboxylic proton to the amino group. Representative snapshots of a BOMD simulation are shown in Fig. 7. The trajectory is included in the SI Movie 7.mp4. Highly polarized hydrogen bonds precede both proton transfers, followed by the stabilization of the U-zwitterion form.

Direct proton transfer from the thiol group to the amino substituent was observed in CG-based geometry optimizations starting from the adsorbed neutral cysteine. As shown in Fig. 8, hydrogen bonds between the thiol and amino groups may result in the transfer of the proton with formation of an ammonium substituent. That the process was observed at 0 K implies that the barrier to direct proton transfer is small. Similar direct (thiol-to-amino) proton transfer processes were observed in cysteine adsorption on surfaces with defects by our group.[66]

Configurational changes in the initial neutral structure inhibited proton transfer, such as when the thiol hydrogen was pointing towards the surface or away from both the amino and the carboxylic groups. On the other hand, no proton transfer in the opposite direction was observed when calculations were initialized with a U-zwitterion motif, including in room temperature BOMD simulations.

3.5 Adsorbed dimers

The discussion above highlights that several adsorbed monomer motifs are competitive in the deposition of cysteine on Au surfaces. Lateral interactions are expected to play important roles at intermediate and high coverage. The nature of these interactions will depend strongly on the specific adsorption motif of each molecule. To explore these issues, we conducted a preliminary investigation of the stability of adsorbed dimers.

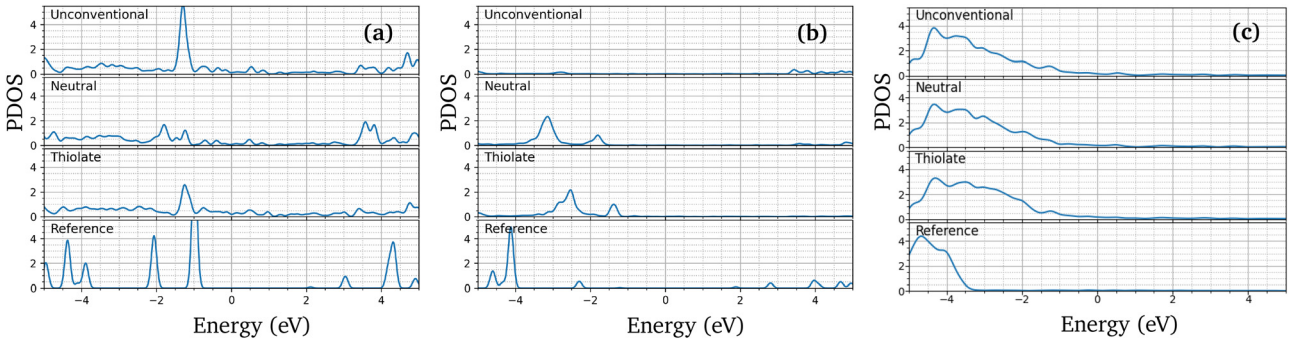

Fig. 6 Projected densities of states for atoms involved in binding of cysteine on gold. Projections are based on electron densities obtained from CG optimizations. Plots for sulfur, nitrogen and closest-bound gold atom-projected DOS are presented in panels (a)–(c), respectively. The complex structures used in the calculations were in the most stable orientation found for each of the three binding modes (U-zwitterionic, neutral, thiolate). The reference is the projected density of states of the sulfur or nitrogen atom in an optimized cysteine monomer that has been moved far away from the surface (~8.5 Å).

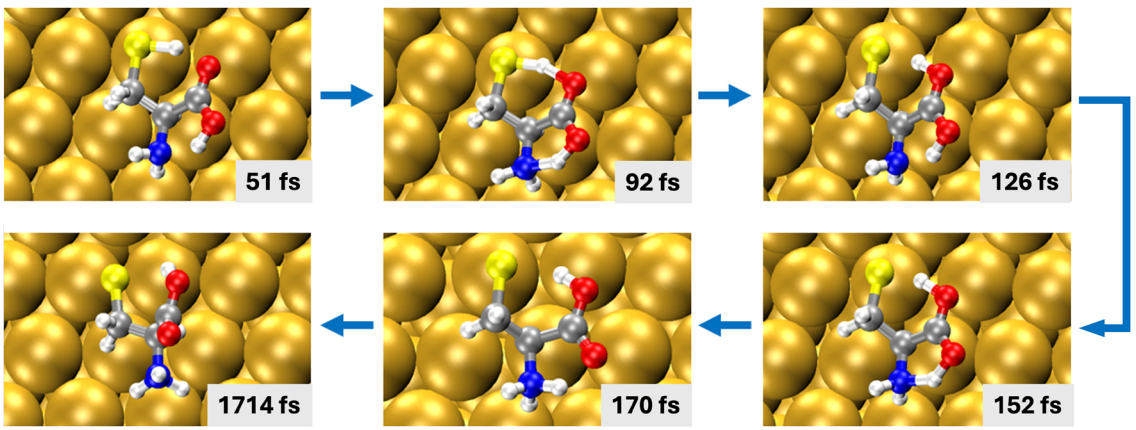

Fig. 7 Representative snapshots along the trajectory of an indirect proton transfer mechanism observed in BOMD calculations. Simulation times corresponding to each snapshot are including in the relevant panels.

The configurational space was sampled through several initial structures, as well as BOMD simulations.

Fig. 9 shows the most stable adsorbed dimer conformations, with energies indicated in Table 2. The most stable dimer had both monomers in the U-zwitterionic form. Moreover, many of these configurations have at least one of the monomers in this form. Nevertheless, the stability of neutral dimers [such as the one presented in Fig. 9(e)] is similar to that of dimers containing U-zwitterionic monomers, consistent with previous DFT calculations of the adsorption energy of neutral dimers.[17] Binding energies are within 0.2 eV per monomer of each other, for all dimer geometries presented in Fig. 9, despite vastly different surface binding and lateral interaction motifs.

Basis set superposition error corrections are more challenging to estimate for adsorbed dimers, as molecules that chemisorb to the surface (*i.e.*, U-zwitterion molecules) will share density with surface orbitals. In these cases counterpoise corrections will likely overestimate this error. Regardless, we obtain corrections between 0.15 and 0.25 eV per molecule, with neutral dimers closer to the higher end of this range. All things considered, the formation of double hydrogen bonds in dimers provide a stabilization energy of roughly 0.3 eV per molecule, in line with previous studies from our group.[16] This cyclic double hydrogen bonding motif has been observed previously in DFT calculations.[8,17] Hydrogen bond lengths in Fig. 9 are less than 1.54 Å and O–H–O bond angles are greater than 174°.

The evolution of optimized dimers under thermal energy (300 K) was followed using BOMD. Starting from the geometries shown in Fig. 9, dimers are highly dynamic at room temperature, with hydrogen bond evolution and/or proton transfer occurring, depending on the initial structure. However, no changes that require the desorption of a group other than

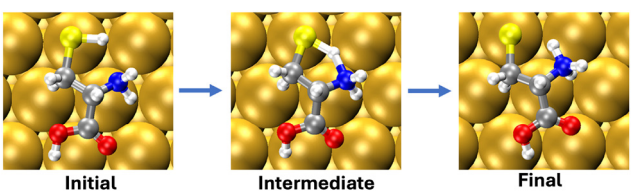

Fig. 8 The initial, intermediate, and final geometries of the direct proton transfer observed in CG-based structural optimization.

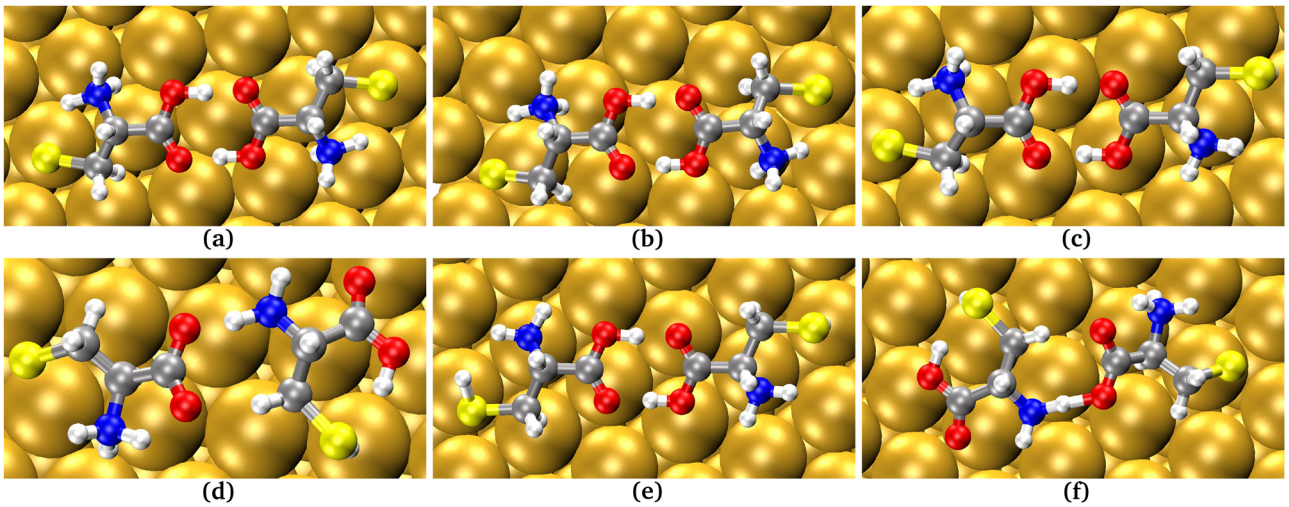

Fig. 9 CG-optimized adsorbed dimer geometries. Corresponding energies can be found in Table 2. Panels (a)–(f) show geometries in order of decreasing binding energy.

Table 2 Adsorption energies of cysteine dimers on the Au(111) surface

Structure[a]	Description	E_b (eV)
Fig. 9(a)	U-zwitterion, U-zwitterion	−1.8
Fig. 9(b)	U-zwitterion, U-zwitterion	−1.7
Fig. 9(c)	U-zwitterion, neutral	−1.7
Fig. 9(d)	U-zwitterion, neutral	−1.7
Fig. 9(e)	Neutral, neutral	−1.6
Fig. 9(f)	U-zwitterion, neutral	−1.6

[a] Entries refer to the optimized structures presented in Fig. 9. Energies presented are per molecule and are calculated from CG-based geometry optimizations using eqn (4).

hydrogen (*i.e.*, torsional motions of the molecular backbone) are observed. A simulation starting from the U-zwitterion dimer shown in Fig. 9(a) mainly shows vibrations in the hydrogen bonds between the carboxylic groups and between the ammonium and thiolate groups (see SI Movie c2.mp4). The U-zwitterion/neutral pair in Fig. 9(c) evolves towards a pair of U-zwitterion molecules *via* hydrogen bond followed by proton donation from the thiol to the amino group (see SI Movie 10.mp4 and Fig. 10). The transformation is again an indication of the stability of U-zwitterion configurations of adsorbed cysteine molecules.

4 Conclusions

We have surveyed neutral, conventionally and unconventionally zwitterionic motifs of cysteine adsorbed on Au(111) substrates, in an effort to gather an understanding of the complex behaviour of this system in a variety of conditions. We found that at low coverage, monomeric conventional zwitterions are unstable before and after adsorption. On the other hand, unconventional zwitterions, in which the mercapto hydrogen is passed to the amino group, are more stable than all other adsorbed motifs.

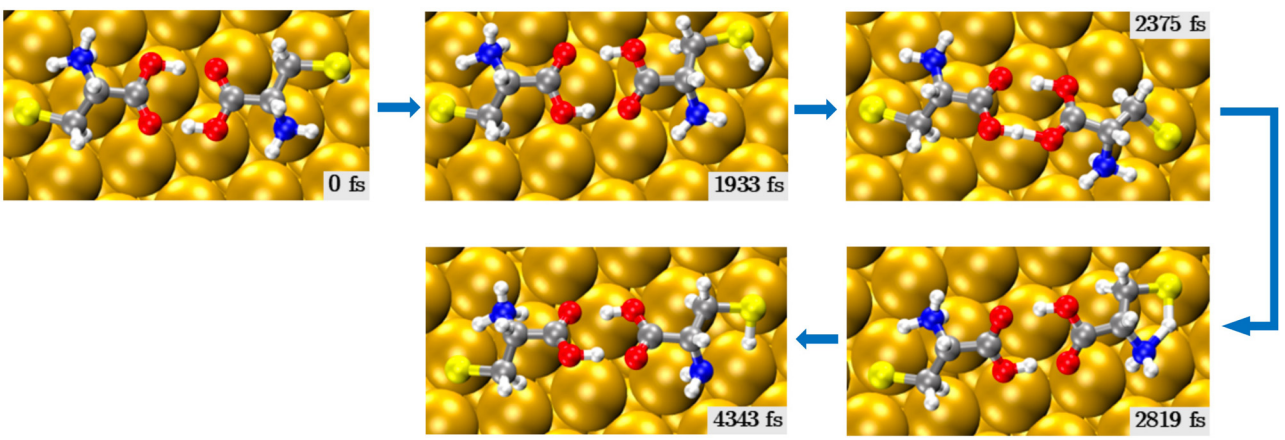

Fig. 10 Room temperature BOMD evolution of an optimized U-zwitterion/neutral dimer. Snapshots showing the direct proton transfer observed in BOMD calculations for a previously dimeric adsorbate are shown for a series of timesteps. Simulation times corresponding to each snapshot are shown directly below each panel.

This is partly related to the stabilization of the sulfur-based anion by bonding to and polarization of the gold surface. Born Oppenheimer molecular dynamics simulations and standard 0 K structural optimization reveal two possible pathways for proton transfer processes: direct sulfur-to-nitrogen or indirect sulfur-to-oxygen-to-nitrogen processes. A systematic investigation of proton transfer mechanisms is currently underway and will be the subject of a future publication. Further stability is achieved in dimers, through formation of hydrogen bonds between carboxylic groups.

Conflicts of interest

There are no conflicts to declare.

Data availability

The data supporting this article have been included as part of the SI. Supplementary information: Structures for all optimized complexes presented herein, as well as simulation trajectories. See DOI: **https://doi.org/10.1039/d5cp01901j**.

Acknowledgements

Funding was provided by NSERC, CFI, BCKDF and the University of Victoria. This research was performed in part using the WestGrid computing resources and the Digital Research Alliance of Canada.

Notes and references

1 J. C. Love, L. A. Estroff, J. K. Kriebel, R. G. Nuzzo and G. M. Whitesides, *Chem. Rev.*, 2005, **105**, 1103–1170.
2 N. K. Chaki and K. Vijayamohanan, *Biosens. Bioelectron.*, 2002, **17**, 1–12.
3 Y. Xia, J. A. Rogers, K. E. Paul and G. M. Whitesides, *Chem. Rev.*, 1999, **99**, 1823–1848.
4 B. Luo, A. Banik, E. W. Bohannan and J. A. Switzer, *J. Phys. Chem. C*, 2020, **124**, 21426–21434.
5 S. Berner, S. Biela, G. Ledung, A. Gogoll, J.-E. Bäckvall, C. Puglia and S. Oscarsson, *J. Catal.*, 2006, **244**, 86–91.
6 M. Canepa, L. Lavagnino, L. Pasquali, R. Moroni, F. Bisio, V. De Renzi, S. Terreni and L. Mattera, *J. Phys.: Condens. Matter*, 2009, **21**, 264005.
7 A. Kühnle, T. R. Linderoth, M. Schunack and F. Besenbacher, *Langmuir*, 2006, **22**, 2156–2160.
8 F. Besenbacher, A. Kühnle, T. R. Linderoth and B. Hammer, *Nature*, 2002, **415**, 891–893.
9 A. Kühnle, T. R. Linderoth and F. Besenbacher, *J. Am. Chem. Soc.*, 2006, **128**, 1076–1077.
10 T. Shin, K.-N. Kim, C.-W. Lee, S. K. Shin and H. Kang, *J. Phys. Chem. B*, 2003, **107**, 11674–11681.
11 L. Caprile, A. Cossaro, E. Falletta, C. Della Pina, O. Cavalleri, R. Rolandi, S. Terreni, R. Ferrando, M. Rossi, L. Floreano and M. Canepa, *Nanoscale*, 2012, **4**, 7727–7734.
12 A. Cossaro, S. Terreni, O. Cavalleri, M. Prato, D. Cvetko, A. Morgante, L. Floreano and M. Canepa, *Langmuir*, 2006, **22**, 11193–11198.
13 R. R. Nazmutdinov, J. Zhang, T. T. Zinkicheva, I. R. Manyurov and J. Ulstrup, *Langmuir*, 2006, **22**, 7556–7567.
14 B. Höffling, F. Ortmann, K. Hannewald and F. Bechstedt, *Phys. Rev. B: Condens. Matter Mater. Phys.*, 2010, **81**, 045407.
15 R. Di Felice, A. Selloni and E. Molinari, *J. Phys. Chem. B*, 2003, **107**, 1151–1156.
16 T. Popa, E. C. Ting and I. Paci, *Surf. Sci.*, 2014, **629**, 20–27.
17 L. Buimaga-Iarinca and A. Calborean, *Phys. Scr.*, 2012, **86**, 35707–35716.
18 Y. Zhao, F. Zhou, H. Zhou and H. Su, *Phys. Chem. Chem. Phys.*, 2013, **15**, 1690–1698.
19 W. Andreoni, A. Curioni and H. Grönbeck, *Int. J. Quantum Chem.*, 2000, **80**, 598–608.
20 W. Miao and A. J. Bard, *Anal. Chem.*, 2003, **75**, 5825–5834.
21 L. Andolfi, A. Bizzarri and S. Cannistraro, *Thin Solid Films*, 2006, **515**, 212–219.
22 H. Wackerbarth, A. P. Tofteng, K. J. Jensen, I. Chorkendorff and J. Ulstrup, *Langmuir*, 2006, **22**, 6661–6667.
23 Z. Ma and H. Han, *Colloids Surf., A*, 2008, **317**, 229–233.
24 A. Majzik, R. Patakfalvi, V. Hornok and I. Dékány, *Gold Bull.*, 2009, **42**, 113–123.
25 Y. Ma, Z. Cao, J. Hao, J. Zhou, Z. Yang, Y. Yang and J. Wei, *J. Phys. Chem. C*, 2020, **124**, 24306–24314.
26 F. Chai, C. Wang, T. Wang, Z. Ma and Z. Su, *Nanotechnology*, 2009, **21**, 025501.
27 H.-E. Lee, H.-Y. Ahn, J. Mun, Y. Y. Lee, M. Kim, N. H. Cho, K. Chang, W. S. Kim, J. Rho and K. T. Nam, *Nature*, 2018, **556**, 360–365.
28 H. Kim, S. W. Im, N. H. Cho, D. H. Seo, R. M. Kim, Y. Lim, H. Lee, H. Ahn and K. T. Nam, *Angew. Chem., Int. Ed.*, 2020, **59**, 12976–12983.
29 G. Dodero, L. De Michieli, O. Cavalleri, R. Rolandi, L. Oliveri, A. Daccà and R. Parodi, *Colloids Surf., A*, 2000, **175**, 121–128.
30 O. Cavalleri, L. Oliveri, A. Daccà, R. Parodi and R. Rolandi, *Appl. Surf. Sci.*, 2001, **175–176**, 357–362.
31 A. Kühnle, T. R. Linderoth and F. Besenbacher, *J. Am. Chem. Soc.*, 2003, **125**, 14680–14681.
32 A. Ihs and B. Liedberg, *J. Colloid Interface Sci.*, 1991, **144**, 282–292.
33 K. Uvdal and T. P. Vikinge, *Langmuir*, 2001, **17**, 2008–2012.
34 G. J. Leggett, M. C. Davies, D. E. Jackson and S. J. B. Tendler, *J. Phys. Chem.*, 1993, **97**, 5348–5355.
35 A. S. Dakkouri, D. M. Kolb, R. Edelstein-Shima and D. Mandler, *Langmuir*, 1996, **12**, 2849–2852.
36 J. Zhang, Q. Chi, J. U. Nielsen, E. P. Friis, J. E. T. Andersen and J. Ulstrup, *Langmuir*, 2000, **16**, 7229–7237.
37 Q.-M. Xu, L.-J. Wan, C. Wang, C.-L. Bai, Z.-Y. Wang and T. Nozawa, *Langmuir*, 2001, **17**, 6203–6206.
38 K. Uvdal, P. Bodö and B. Liedberg, *J. Colloid Interface Sci.*, 1992, **149**, 162–173.

39 C. Vericat, M. E. Vela, G. Benitez, P. Carro and R. C. Salvarezza, *Chem. Soc. Rev.*, 2010, **39**, 1805–1834.
40 A. Abraham, A. J. Ilott, J. Miller and T. Gullion, *J. Phys. Chem. B*, 2012, **116**, 7771–7775.
41 N. B. Luque and E. Santos, *Langmuir*, 2012, **28**, 11472–11480.
42 E. Ataman, C. Isvoranu, J. N. Andersen, J. Schnadt and K. Schulte, *J. Phys. Chem. Lett.*, 2011, **2**, 1677–1681.
43 M. D. Hanwell, D. E. Curtis, D. C. Lonie, T. Vandermeersch, E. Zurek and G. R. Hutchison, *J. Cheminf.*, 2012, **4**, 17.
44 **https://github.com/cryos/avogadro/blob/master/crystals/elements/Au-Gold.cif**.
45 **https://rruff.geo.arizona.edu/AMS/amcsd.php**.
46 J. M. Soler, E. Artacho, J. D. Gale, A. García, J. Junquera, P. Ordejón and D. Sánchez-Portal, *J. Phys.: Condens. Matter*, 2002, **14**, 2745–2779.
47 C. Chapman and I. Paci, *J. Phys. Chem. C*, 2010, **114**, 20556–20563.
48 T. Popa and I. Paci, *J. Phys. Chem. C*, 2015, **119**, 9829–9838.
49 J. P. Perdew, K. Burke and M. Ernzerhof, *Phys. Rev. Lett.*, 1997, **78**, 1396.
50 A. Tkatchenko and M. Scheffler, *Phys. Rev. Lett.*, 2009, **102**, 073005.
51 N. Troullier and J. L. Martins, *Phys. Rev. B: Condens. Matter Mater. Phys.*, 1991, **43**, 1993–2006.
52 K. Lee, J. Yu and Y. Morikawa, *Phys. Rev. B: Condens. Matter Mater. Phys.*, 2007, **75**, 045402.
53 C. R. L. Chapman, E. C. Ting, A. Kereszti and I. Paci, *J. Phys. Chem. C*, 2013, **117**, 19426–19435.
54 S. Boys and F. Bernardi, *Mol. Phys.*, 1970, **19**, 553–566.
55 D. Dissanayake, Y. Hassan, E. Tuca and I. Paci, *J. Phys. Chem. C*, 2023, **127**, 14999–15010.
56 E. C. M. Ting, T. Popa and I. Paci, *Beilstein J. Nanotechnol.*, 2016, **7**, 53–61.
57 L. Leiserowitz, *Acta Crystallogr., Sect. B*, 1976, **32**, 775–802.
58 A. Gavezzotti, *Acta Crystallogr., Sect. B: Struct. Sci.*, 2008, **64**, 401–403.
59 D. S. Middlemiss, M. Facchini, C. A. Morrison and C. C. Wilson, *CrystEngComm*, 2007, **9**, 777.
60 B. A. Kolesov, V. S. Minkov, E. V. Boldyreva and T. N. Drebushchak, *J. Phys. Chem. B*, 2008, **112**, 12827–12839.
61 S. Gómez, S. Gómez, J. David, D. Guerra, C. Cappelli and A. Restrepo, *Molecules*, 2022, **27**, 8665.
62 B. Hammer and J. Nørskov, *Adv. Catal.*, 2000, **45**, 71–129.
63 C. F. Dickens, J. H. Montoya, A. R. Kulkarni, M. Bajdich and J. K. Nørskov, *Surf. Sci.*, 2019, **681**, 122–129.
64 L. Qingwen, G. Hong, W. Yiming, L. Guoan and M. Jie, *Electroanalysis*, 2001, **13**, 1342–1346.
65 M. Honda, Y. Baba, N. Hirao and T. Sekiguchi, *e-J. Surf. Sci. Nanotechnol.*, 2009, **7**, 110–114.
66 A. Idris, C. Smith, C.-M. Ting and I. Paci, *J. Phys. Chem. C*, 2025, **129**, 13992–14001.

